Dynamic Behavior in Laser Gas Cutting of Mild Steel†

Yoshiaki ARATA*, Hiroshi MARUO**, Isamu MIYAMOTO*** and Sadao TAKEUCHI****

Abstract

Mechanism for the laser gas cutting mild steel with oxygen jet is discussed based on information including the cut appearances, high speed color films of the cutting behavior, power density distribution of the focused laser beam and temperature distribution at the cutting front. At the cutting speed Vb below cirtical one, 2 m/min, which is independent of the laser power, the cutting phenomena are found to vary periodically because the reaction speed at the cutting front is faster than V_b by activation of the intense laser beam. At speeds higher than 2 m/min, the cutting phenomena become steady and the high temperature produced by high power density of the beam povides high speed cutting, which could not be achieved in the conventional oxy-acetylen gas cutting. The effect of such periodic cutting phenomena on the quality of the cut is described and conditions available for qualified cuts are recommended.

KEY WORDS: (Laser Gas Cutting) (Oxidation) (Mild Steel) (Mechanism) (High Speed Filming) (Temperature) (Beam Power Density) (Quality)

1. Introduction

In principle most materials can be cut by focused laser beam through melting or vaporization due to its high power density. In ferrous materials the addition of O_2 gas jet to the laser cutting has been shown to extremely improve the cutting performances because of the high beam absorptivity of the oxide film, the highly concentrated exothermic energy released in the reaction zone, and the low melting temperature and the high fluidity of oxide slag.[1] [2] Such a cutting method, which is referred to as "the laser gas cutting", has been much noticed because it provides so high quality and so high speed cuts that the conventional oxy-acetylen cutting cannot achieve.

A substantial amount of work has been performed on the laser gas cutting, demonstrating its feasibility. [3] ~ [12] However, in spite of potential capability of the laser gas cutting, few industrial applications have been reported. This is thought to be caused by the absence of a detailed, systematic investigation into the mechanism for the laser gas cutting which may reveal how the cuts are affected by the parameters including the beam power density, the cutting speed and the thickness of plate. As for the cutting mechanisms, the interaction between the focused laser beam and material to be cut has to be revealed. This includes the three-dimensional motion of the cutting front, behavior of molten material and the temperature of the reaction front as a function of the cutting speed.

Two-dimensional behavior of the cutting front[13] has been inferred based on high speed films taken with edge cutting which machines a thin slice from the workpiece, thereby periodic phenomena have been found to occur in the laser gas cutting.

In the present study, a new filming technique which enables one to observe the practical cutting has been introduced reproducing the three-dimensional motion of the cutting front precisely. The mechanism of the laser gas cutting has been discussed based on this information, the power density distribution in the focused laser beam spot and the temperature distribution in the cutting front. The effect of those phenomena on the quality of the cuts is also discussed.

2. Experimental Procedures

The data presented were obtained by using two continuous wave CO_2 lasers; one is a proto-type 200 W CO_2 laser and another CO_2 gas transport laser with the maximum output of 1.5 KW, GTE Sylvania, Inc. Model 971.

† Received on October 5, 1979
* Professor
** Professor, Faculty of Engineering, Osaka University
*** Research Instructor, Faculty of Engineering, Osaka University
**** Research Student

Transactions of JWRI is published by Welding Research Institute of Osaka University, Suita, Osaka, Japan

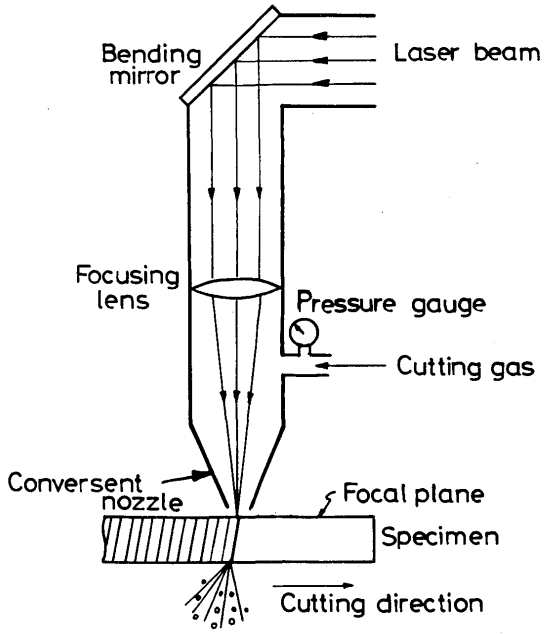

Fig. 1 Schematic diagram of laser gas cutting head.

The laser beam was focused onto the workpiece surface through a ZnSe lens with a focal length of 100 mm as shown in **Fig. 1**. The cutting experiments were carried out by directing the laser beam and oxygen gas coaxially through a convergent nozzle with 1.5 mm diameter, and by moving the workpiece, structural mild steel, SS41.

High speed color films were taken at 4000 frames/sec. The high speed movie camera was set so as to observe directly the leading face of the cut at an angle of about 30° downwards to the workpiece surface as illustrated in **Fig. 2(a)**. By this filming arrangement, suitable to observe

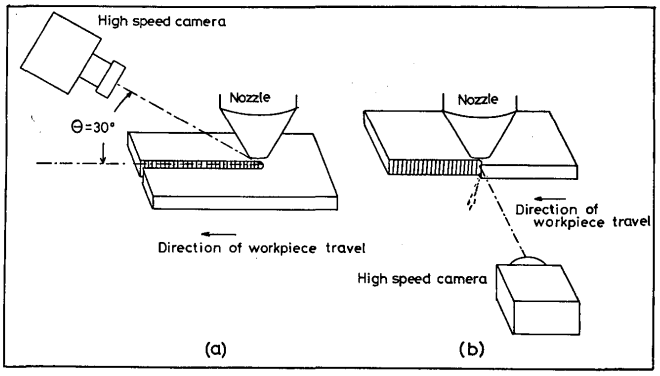

Fig. 2 Arrangement for high speed filming of laser gas cutting
(a) For normal cutting (b) For edge cutting.

both vertical and lateral motions of the cutting front, the motion of the cutting front in the proceeding direction at the workpiece surface can also be observed. We also supplementally carried out filming with the camera perpendicular to the cut and with the edge cutting, which machines a thin slice from the workpiece edge, as shown in **Fig. 2(b)**. Motion of the cutting front was analyzed primarily from the films taken by the former technique and supplementally by the later.

The temperature in the cutting front was measured by means of a radiation pyrometer, which was set in stead of the high speed camera shown in **Fig. 2(a)**. Since the width of the laser gas cuts was generally narrower than a minimum sensing spot diameter, 0.6 mm, of the radiation pyrometer, the temperature observed was calibrated as follows. The temperatures of a tungsten ribon lump were measured by the pyrometer with and without a slit having same width as the cut width to obtain temperature reading-ratio.

3. Experimental results

3.1 Beam power density distribution

A power meter was arranged just below a copper plate with a sharp edge which moved in the x direction as shown in **Fig. 3**, and the power was recorded as a function

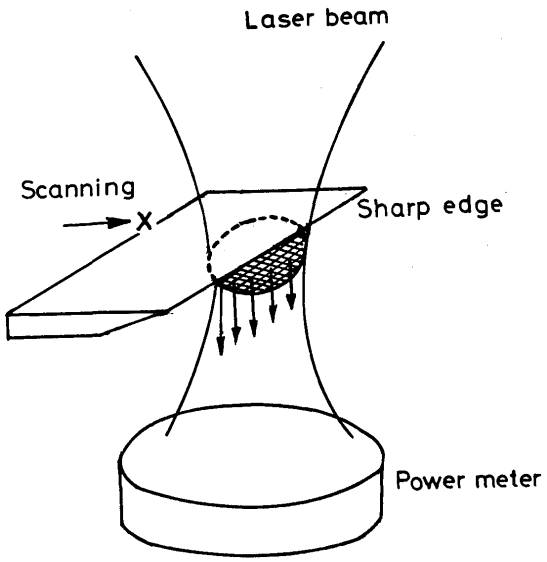

Fig. 3 Arrangement for measurment of power density distribution in focused beam.

of x. The beam power density distribution was determined by differentiating the power with respect to x, and by Abel inversion.

Figure 4 shows the power density profile in the focal plane of the laser beam of the 200 W laser. This profile can be approximated by a Gaussian curve with a radius 0.1 mm at which the intensity falls to 1/e of the center, and the maximum power density at the axis was about 5 x 10^5 W/cm^2 at 200 W power level.

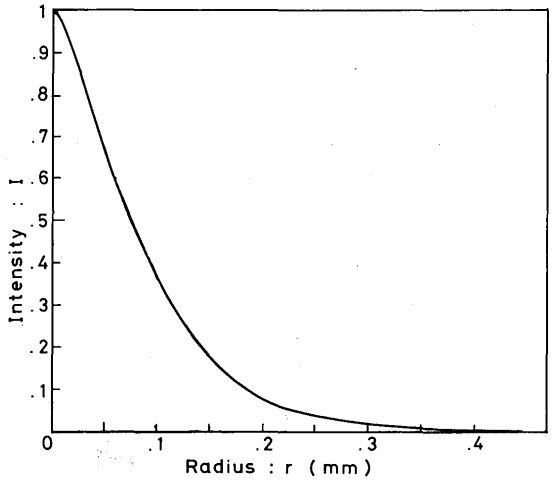

Fig. 4 Radial intensity distribution of laser beam on focal plane.

3.2 Cross-section and edge of the cuts

In the laser O_2 gas cutting of mild steel, the cross-sections are significantly affected by the cutting speed V_b, and are classified into five groups as shown in **Fig. 5**. At

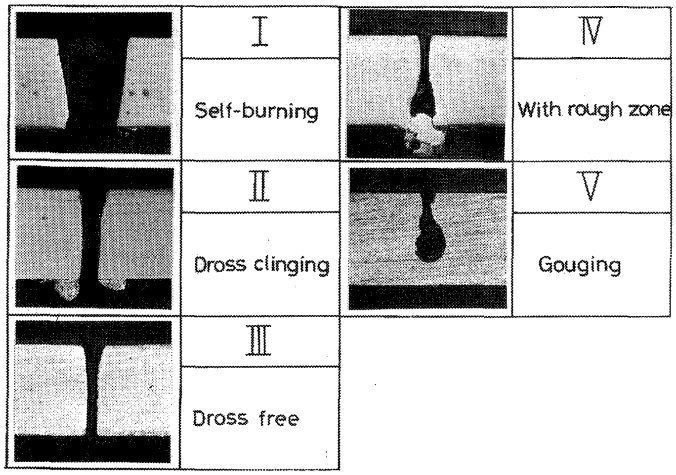

Fig. 5 Classification of laser gas cuts based on shape of cross section.

very low speeds, the cuts contain irregularly spaced holes of which diameter are much larger than the beam spot size and hence are of irregular width. These rough cuts, group I, are referred to as self-burning cuts. At higher speeds, the almost parallel sided cuts, group II and III, with smooth surfaces and narrow kerf width comparable to the beam spot size, are obtianed. Cuts III can be distinguished from the cuts II by no dross attached to the rear surface of the workpiece. More increase in the cutting speed produces group IV cuts of which kerf is wider and irregular at the lower part, and the upper retained as smooth as group III. The appearance at the lower part

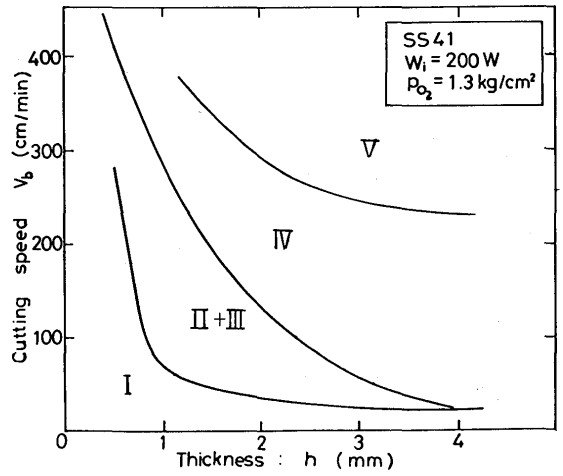

(a) 200 W power level

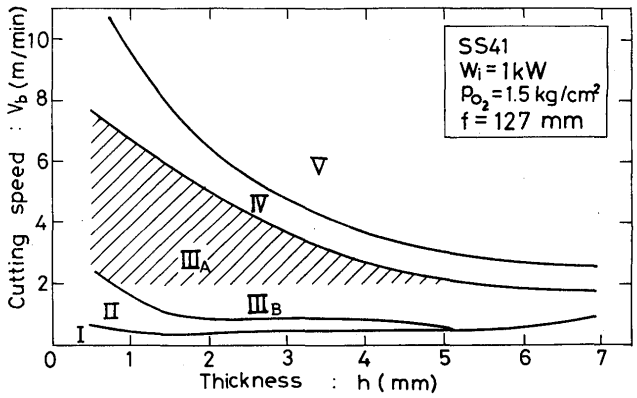

(b) 1 KW power level

Fig. 6 Effect of cutting speed and plate thickness on cut quality.

for the group IV is a sympton of a lack of laser power there.[11] At still higher speeds, cutting-off becomes impossible as in group V. Only the cuts, groups II and III, are available for practical cutting application. **Figure 6** shows the these quality regions in thickness-speed diagram obtained at 200 W and also 1 KW power levels. At higher power level, II and III regions spread to higher speed and larger thickness sides. At 1 KW power level, for example, 0.8 mm thick plate can be cut at 7 m/min, which is much faster than the conventional oxyacetylen cutting, about 2 m/min at most. **Figure 7** demonstrates

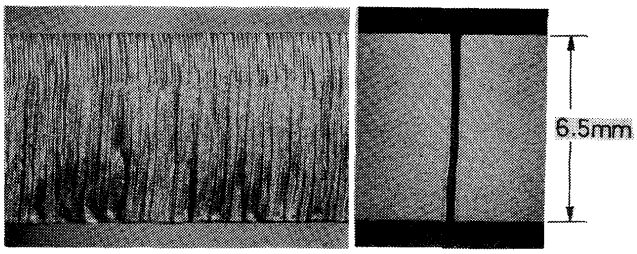

Fig. 7 Example of the laser gas cut. (thickness : 6.5 mm, laser power : 1 KW, cutting speed : 100 cm/min, focal length : 127 mm)

an example of high quality cut of 6.5 mm thickness with very narrow kerf, about 0.25 mm, and very thin heat affected zone.

In the regions II and III, the roughness of the cut surface is one of the important factors for evaluating the cut quality, and so the cut surface was examined in detial. **Figure 8** shows the cut surfaces of 1.2 mm thickness for

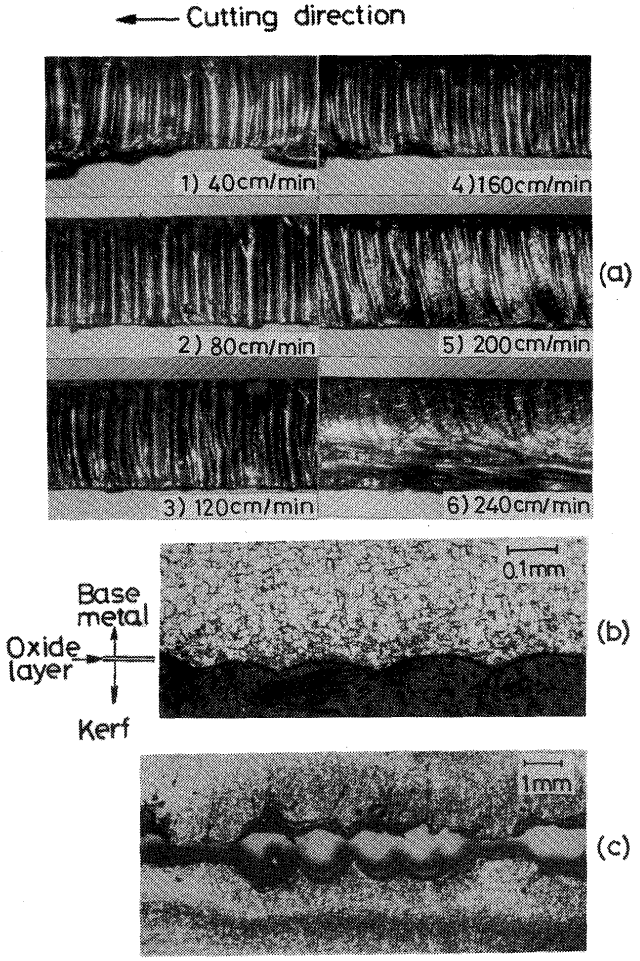

Fig. 8 Cut appearances at 200 W power level. (thickness : 1.2 mm, oxygen pressure ; 1.3 kg/cm^2) (a) Cut surface
(b) Contour of cut surface (cutting speed ; 80 cm/min)
(c) Example of self-burning cut (cutting speed : 10 cm/min)

various cutting speeds at 200 W power level. The cut surfaces at a speed range below 200 cm/min show a series of regularly spaced striations. In detail, the cut surface has a contour with circular arcs and raised ridges as shown in **Fig. 8(b)** and is covered with very thin oxide layer, less than 10μm in thickness, without any symptons of the melted metal layer.

On the other hand, the cut surfaces of 3 mm thickness obtained at 1 KW power level exhibit the regularly spaced striations only in the upper portion accompanied by rather irregular striations in the lower portion as shown in **Fig. 9.**

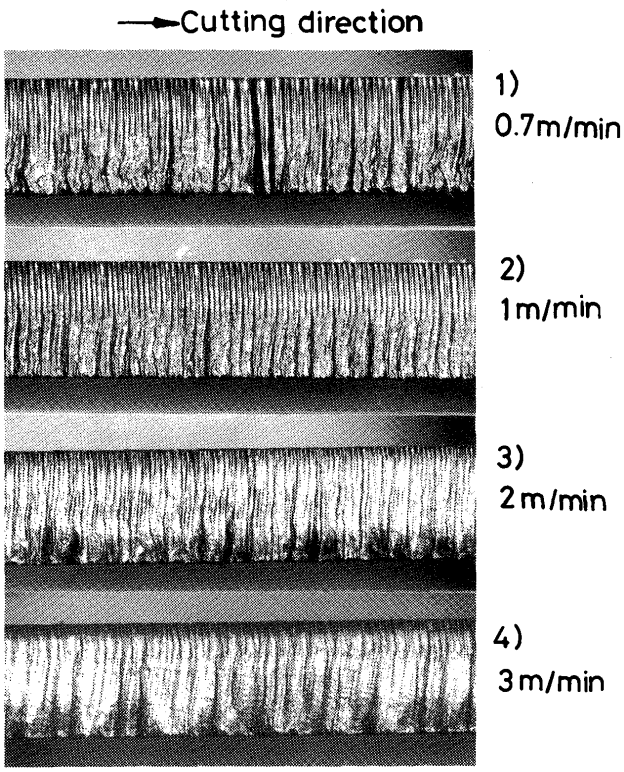

Fig. 9 Appearances of cut surface at 1 KW. (thickness : 3 mm, oxygen pressure : 1.5 kg/cm^2, focal length ; 127 mm)

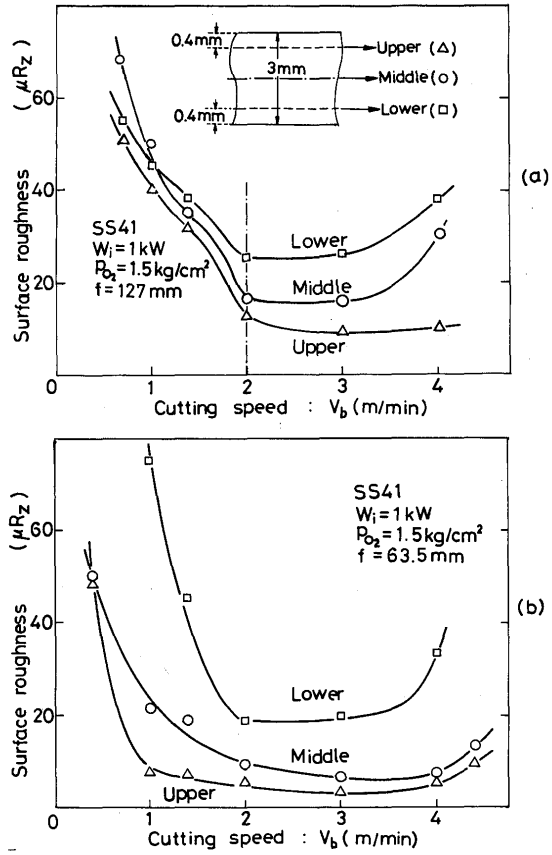

Fig. 10 Roughness of cut surface at 1 KW in terms of ten point height as a function of cutting speed.
(a) Focal length : 127 mm
(b) Focal length : 63.5 mm

Figure 10 shows the roughness of the cut surface in terms of ten points height measured at various locations of 3 mm thick plate. The roughness of the upper portion tended to decrease with increasing the cutting speed until it became constant value, about $10\mu R_z$, at speeds of $V_b >$ 2 m/min. The roughness at the middle and lower parts varied with similar tendency to the upper one.

3.3 Dynamic behavior of the cutting front

In the early stage of the work, filming was carried out with the edge cutting shown in **Fig. 2(b)**. In the edge cutting, however, the cut appearances were found to be significantly dependent on the thickness of the slice machined from the workpiece. With the selected thickness of the machined slice, the cut appearances became similar to those of normal cuts except for the lower part of the cut which became less regular as shown in **Fig. 11**. Although the thickness of the slice was too large to observe the behavior of the cutting face in front of the beam axis, the upper part of the edge cut gave some auxiliary information on the mechanism for the laser gas cutting. The problem that occurred in the edge cutting was resolved by introducing the filming technique shown in **Fig. 2(a)** which enables the camera to observe the behavior of the normal cutting front.

High speed filming was carried out with the arrangement shown in Fig. 2(a) in a cutting speed range from 40 cm/min to 300 cm/min. The films showed that the cutting phenomena in the speeds range below 2 m/min changed periodically with a same frequency as that of the striations left on the cut surfaces shown in **Fig. 8**, and that the cutting phenomena became almost steady at the speeds above 2 m/min.

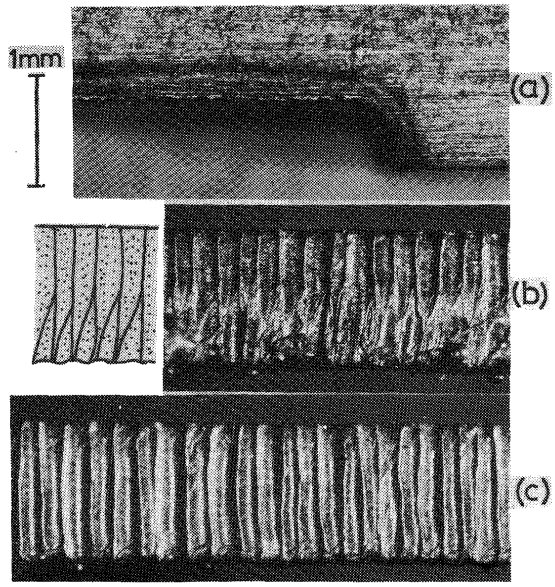

Fig. 11 Comparison between edge cut and normal cut. (thickness : 1.2 mm, cutting speed : 80 cm/min)
(a) Top view of edge cut
(b) Surface of edge cut
(c) Surface of normal cut

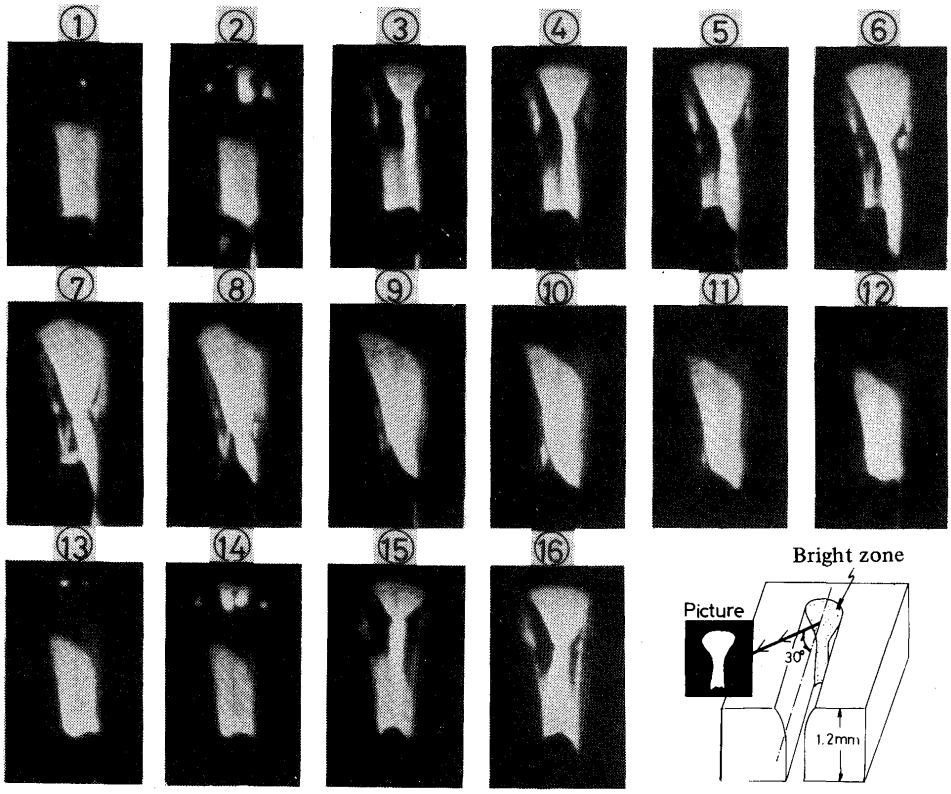

Fig. 12 High speed movie pictures of normal cutting at 80 cm/min (thickness : 1.2 mm, laser power : 200 W). Time interval of each picture is 1/1000 sec.

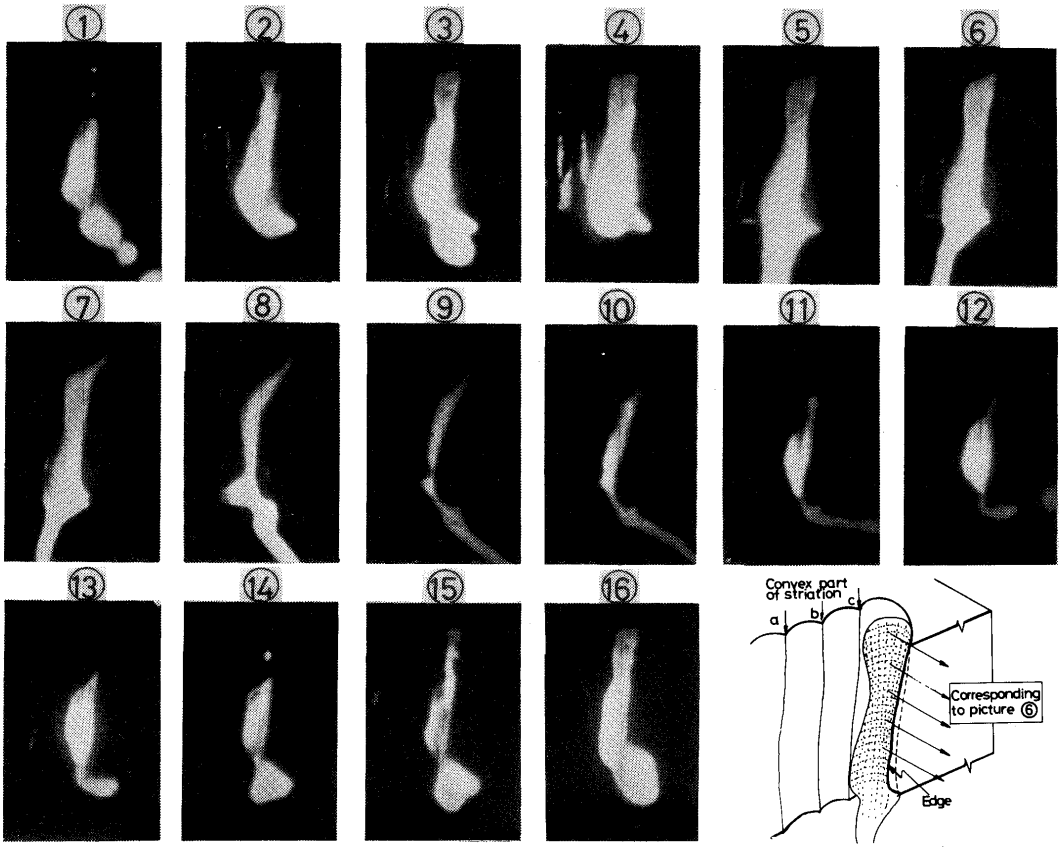

Fig. 13 High speed movie pictures of edge cutting at 80 cm/min (thickness : 1.2 mm, laser power : 200 W). Time interval of each picture is 1/1000 sec.

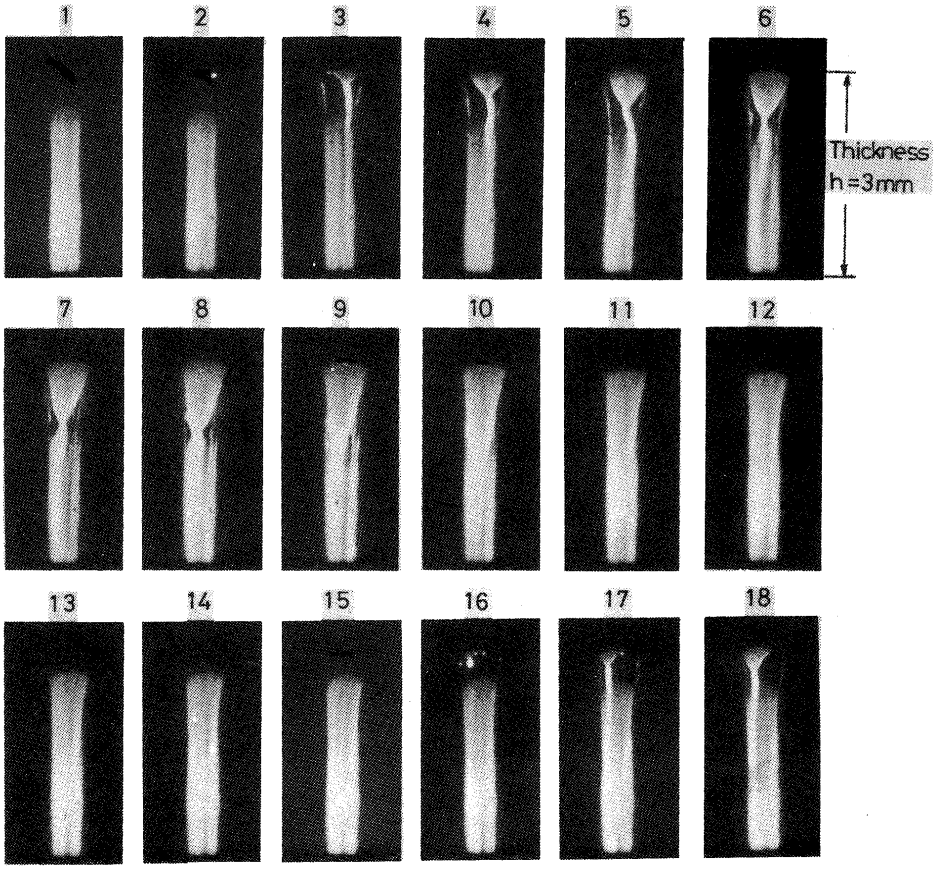

Fig. 14 High speed movie pictures of normal cutting at 100 cm/min (thickness : 3 mm, laser power : 1 KW). Time interval of each picture is 1/1000 sec.

Figure 12 shows a typical example of periodic cutting phenomena, at the laser power level of 200 W. It is seen in this figure that the cutting phenomena at the upper part are periodic whereas at the lower part almost steady. The phenomena observed in one cycle were as follows: an isolated bright spot appeared at the top of the cuutting front and was seen to spread laterally and downwards to grow into an inverted triangle. In the process of growth of the triangle the molten material poured down through the bottom corner. It was also found that the top of the cutting front spread upwards slightly in this stage. After growing up, the triangular zone moved downwards and eventually the upper part lost its brightness completely. Although the shape of the bright area at the lower part hardly changed, the brightness itself changed correspondingly to the periodic change at the upper part.

Figure 13 shows the corresponding behavior of the cutting front observed in the edge cutting. The growth and downward motion of the triangular reaction zone observed in **Fig. 12** corresponded to the change in the width of the melt flow in the direction of the cutting near the top surface of the plate observed in **Fig. 13**. The molten material is, however, seen to flow down unsmoothly causing less regular striations at the lower part.

At the power level of 1 KW, the cyclic phenomena at the upper part could be more clearly observed as shown in **Fig. 14**.

Such cyclic cutting phenomena were observed only at speeds V_b<2m/min. An increase in the speed V_b decreased the intensity of the cyclic change until almost steady cutting was established at V_b=2 m/min; at 2 m/min a very little change in brightness only at the both sides of the cutting front was observed. At 3 m/min, the cutting was completely steady as shown in **Fig. 15**.

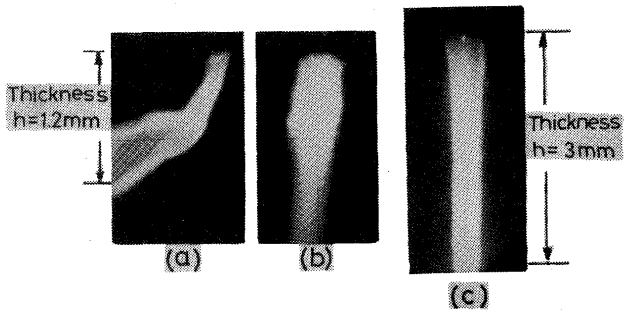

Fig. 15 Example of steady cutting.
(a) Edge cutting at 300 cm/min (200 W)
(b) Normal cutting at 300 cm/min (200 W)
(c) Normal cutting at 250 cm/min (1 KW)

3.4 The reaction speed

Four values, l_r, l_s, l_n and l_w, shown in **Fig. 16**, which were important parameters characterizing three-dimensinal motion of the triangular reaction zone, were measured from the films. The origion of the Cartesian coordinate which moved at a constant velocity V_b was set at the point where a bright spot appeared at the top of the cutting front.

Although these values exhibited a scatter to some extent, they were found to be obviously affected by the cutting speed V_b. In **Fig. 16(b)** and **(c)**, the time variations of these values in typical cycles are plotted for V_b=80 cm/min and V_b=140 cm/min. The maximum value of l_r, which is the amplitude of the cyclic motion of the cutting front in the direction of cutting, was found to decrease with increasing the cutting speed V_b; 0.1 mm at 40 cm/min, 0.09 mm at 80 cm/min and 0.06 mm at 140 cm/min.

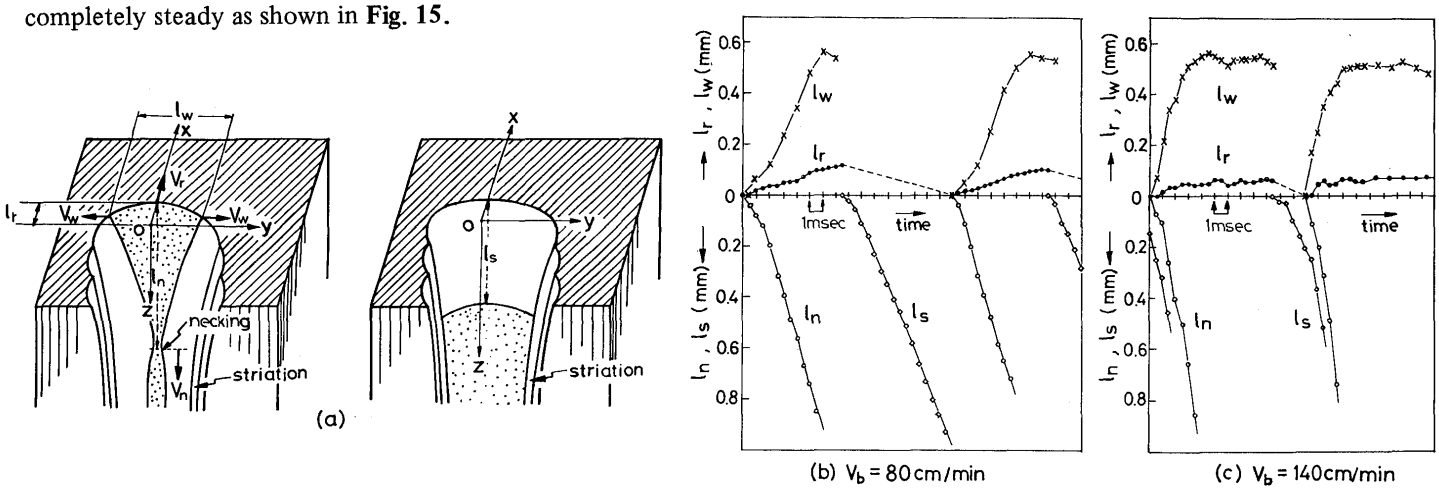

Fig. 16 Time variations of bright zone seen in upper part of cutting front in shape which are characterized by four dimensions and corresponding four velocities.
(a) Each dimension
(b) Data for 80 cm/min
(c) Data for 140 cm/min

From **Fig. 16**, mean velocities V_w, V_r, V_n and V_s were obtained. The velocities V_n, V_s and V_w increased with increasing the cutting velocity V_b, whereas V_r remained almost at contant value, V_{r0}, about 2 m/min, at speed range V_b<2m/min as shown in **Fig. 17**. In a speed range $V_b \gtrsim 2$ m/min, V_r coincided with V_b in consequence of steady cutting.

As shown in **Fig. 18(b)**, the oxidation reaction started at a point S was found to continue with the aid of the laser heating until a point F was reached, where S and F are the location at the distance D_S and D_F from the beam axis, and $D_F - D_S$ is equal to the maximum value of l_r in **Fig. 16**. The distance D_F was measured during cutting by means of a telescope as shown in **Fig. 18(a)**, and the value $D_F - D_S$ was determined from **Fig. 16**. The values D_F and D_S thus obtained are plotted against the cutting speed at power level of 200 W in **Fig. 18(c)**.

Two beam power densities, ϵ_S and ϵ_F, corresponding to S and F respecively, were also determined from the beam power density profile in Fig. 4; ϵ_S and ϵ_F are the power density of the laser beam with which oxidation reaction begins and interrupts, respectively. As shown in **Fig. 18(d)**, at speeds $V_b < 2$ m/min, ϵ_S was almost kept constant at about 6 x 10^4 W/cm^2, whereas ϵ_F increased with increasing V_b until it coincides with ϵ_S at V_b=2 m/min. At speeds $V_b > 2$ m/min, ϵ_S increased with V_b. It is believed that the cutting seed can be increased until ϵ_S reaches the maximum power density at the beam axis, 5 x 10^5 W/cm^2 at 200 W power level, as far as concerned with thin material.

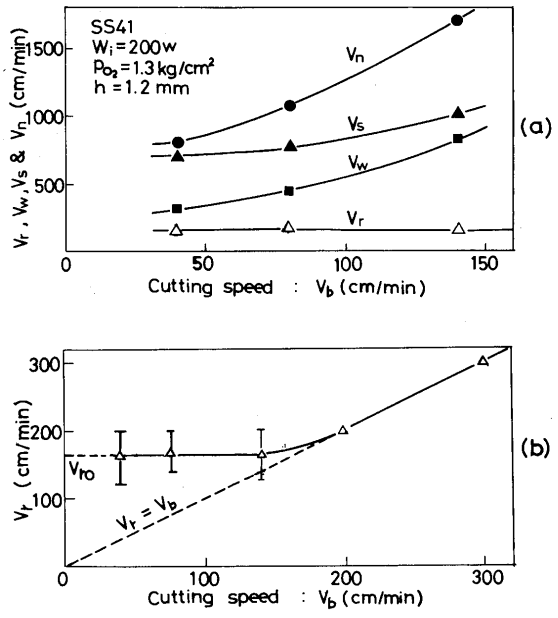

Fig. 17 Relationship between cutting speed and each speed.

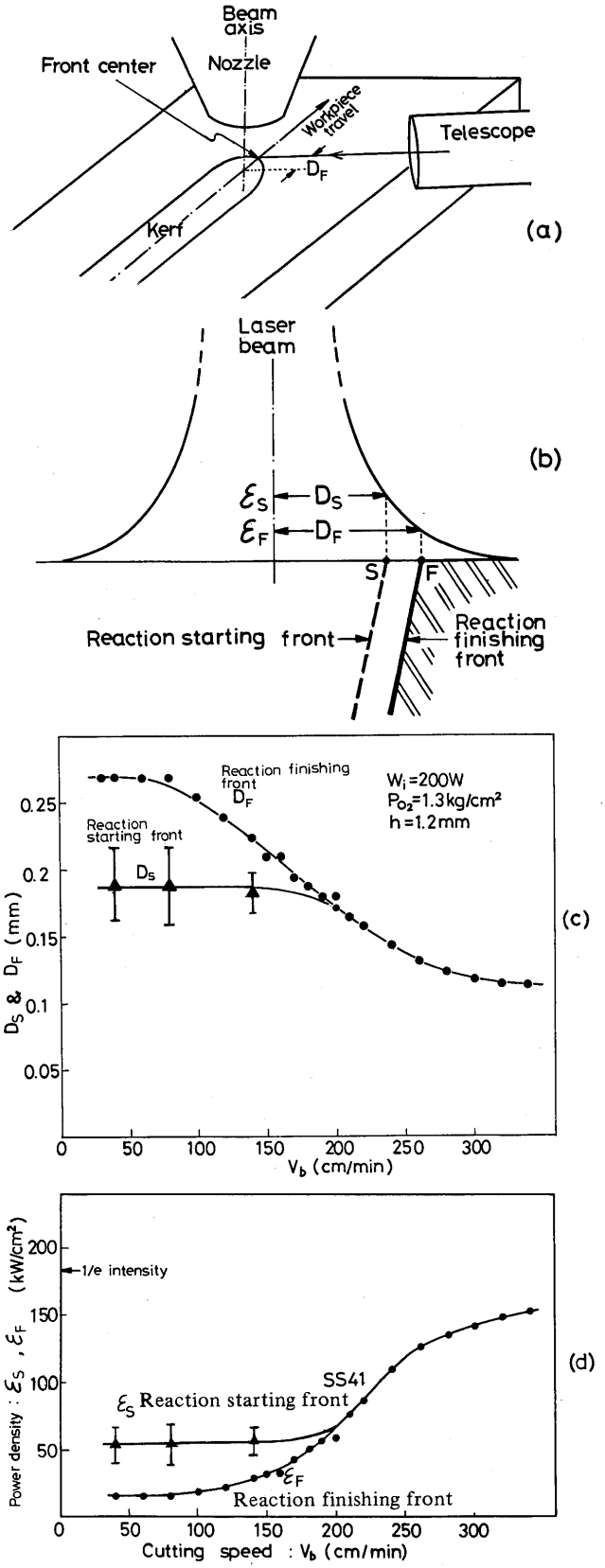

Fig. 18 Locations of reaction starting and finishing points S and F, and corresponding power densities, ϵ_S and ϵ_F.
(a) Arrangements for measuring location of F
(b) Reaction starting and finishing fronts, D_S and D_F distant from beam axis, respectively
(c) Effect of cutting speed on D_S and D_F
(d) Effect of cutting speed on beam power densities ϵ_S and ϵ_F which correspond to D_S and D_F, respectively

3.5 Temperature at the cutting front

Figure 19 indicates the temperature distributions along the z axis. The temperature tended to increase with increasing the distance from the top surface z until the constant temperature distribution is established.

At 1 m/min the region where the temperature increased with z corresponded to the region where periodic cutting phenomena were observed, and the region showing constant temperature distribution corresponded to the part where the rather irregular striations were observed in the lower portion shown in **Fig. 9.** At 4 m/min, the region where the temperature decreased with z was seen to occur. In this region the cut appearances were extremely rough. This is caused by the fact that the laser energy supply is not enough to produce a clear cut [11] because the cutting speed is too high.

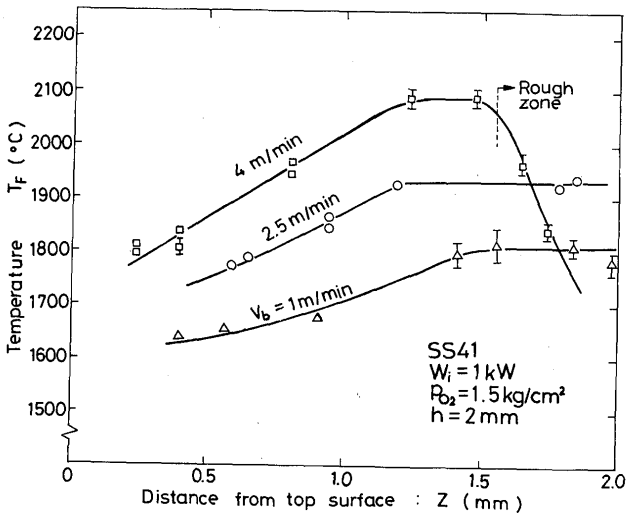

Fig. 19 Relationship between temperature of cutting front and distance from top surface for various cutting speeds.

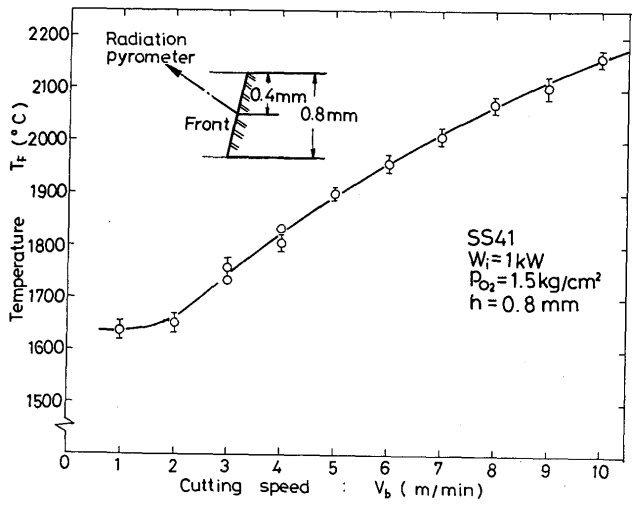

Fig. 20 Relationship between cutting speed and temperature.

Figure 20 exhibits the relationship between the temperature at the cutting front and the cutting speed. At speeds below 2 m/min, the temperature was almost constant, about 1650°C, which corresponds to that of oxy-acetylen cutting.[14]-[16] At speeds above 2 m/min, the temperature increased directly with the speed. The maximum temperature, 2150°C, was obtained in our experiment at V_b=10 m/min, which is the upper limit of the carriage used. It is believed that as the cutting speed increases further, the temperature at the cutting front will reach to the evaporation temperature.

4. Discussion

4.1 Mechanisms for laser gas cutting

The mechanisms for the laser gas cutting mild steel were discussed based on information including the cut apperances, the beam power density distribution, and the periodic motion and temperature obtained at the cutting front under various operating conditions. The prosposed interactions between the laser beam and the cutting front are illustrated in **Figs. 21, 22** and **23.**

Figure 21(a) exhibits the top view of model proposed to explain periodic cutting observed at the cutting speeds below 2 m/min. The circles O_S and O_F, of which centers are P_S and P_F, are equipower density circles with ϵ_S and

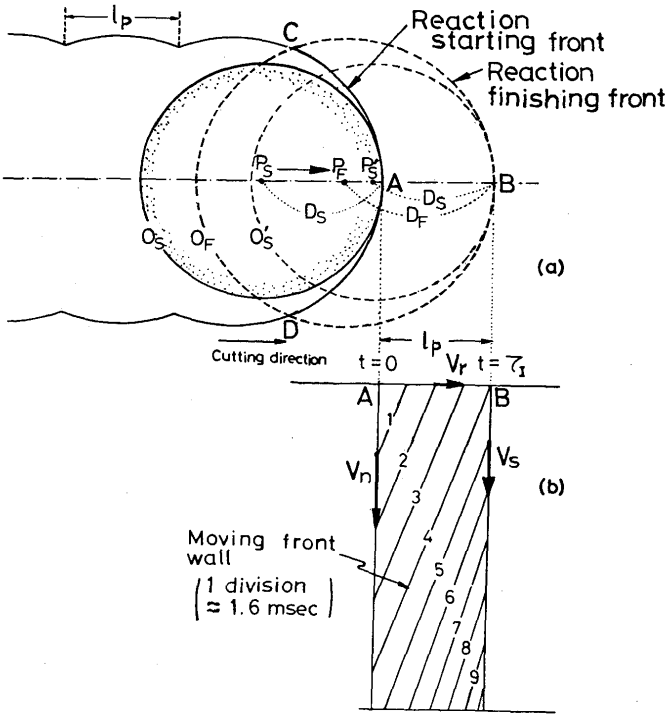

Fig. 21 Model showing periodically changing cutting.
(a) Top view
(b) Longitudinal cross section of cutting front of thin plate

ϵ_F, respectively. On coming in contact with the edge of the face CAD, the circle 0_S with the reaction starting power density ϵ_S, triggers off the oxidation reaction. The reaction front moves along the x-axis at V_r which is faster than V_b until it reaches the circle O_F with the reaction finishing power density, ϵ_F. In this process oxidation reaction spreads laterally so that the region CADB is removed. Then no action follws until the circle O's reaches the cutting front at B again. Thus a circular arc and a ridge at C are left. **Figure 21(b)** shows the corresponding behavior in the longitudinal cross section.

Figure 22 illustrates the time varing longitudinal cross section of the cutting front in the periodic cutting thick plate. When the circle O_S comes in contact with the cutting front, the isolated bright spot appears since the cutting front at the upper part is near vertical, whereas the lower part is constantly heated by the laser beam. As the spot grows into the triangle the upper part is removed so as to have an inclined face, and then the melt from the upper part pours into the lower part. Although the striations in the both parts are produced in a different way each other, the amount of the melt and hence energy included in the lower part is affected by the upper phenomena as shown in **Fig. 10**. Such an intermittent cutting is caused by the fact that the velocity of the reaction front, V_{r0}, activated by the laser beam with the power density ϵ_S is faster than the cutting speed V_b.

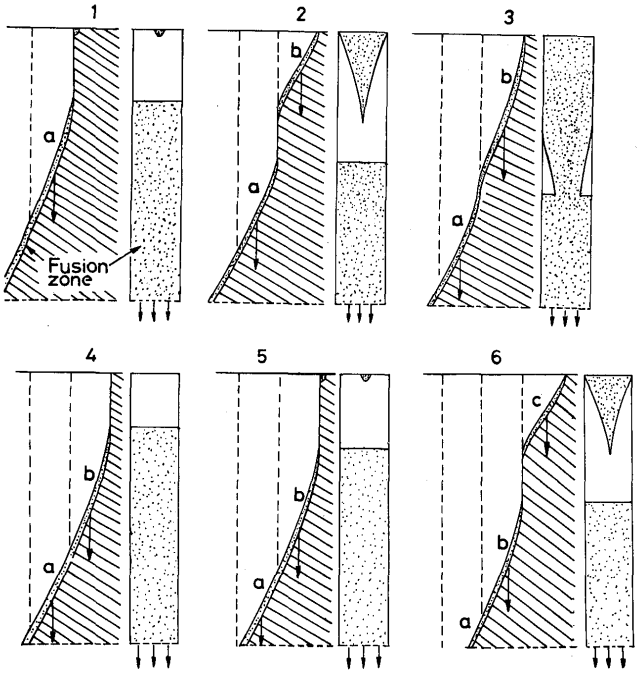

Fig. 22 Schematic illustration showing periodically changing cutting behavior of thick plate in longitudinal cross section.

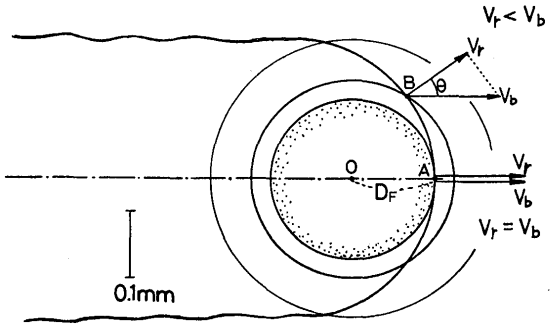

Fig. 23 Schematic illustration showing steady cutting.

At the cutting speed $V_b=V_{r0}$, the cutting becomes steady leaving no obvious striations on the cut surfaces, since the circle of ϵ_S is always in contact with the cutting front. At the cutting speeds higher than V_{r0}, increase in the density ϵ_S has an effect to raise the temperature of the cutting front so as to enhance the reaction velocity up to V_b keeping the steady cutting. Such a high speed cutting which could not be achieved by the conventional oxy-acetylen cutting is due to the high power density which was realized by the laser beam.

At the very low cutting speeds, the cuts with the self-burning shown in **Fig. 8(c)** occurred which contains irregularly spaced holes with a diameter much larger than the beam spot size as described already. The oxidation reaction then will spread out beyond the circle of the reaction finishing power density ϵ_F, because the thermal conduction becomes predominant in the temperature distributions. This effect will be accelerated by the large amount of heat contained within the dross which easily deposits to the bottom surface of the thin plate in low speed cutting.

The kerf width at any cutting speeds should be also affected by the thermal conduction; in general moving heat sources provide isothermal lines of which maximum width is larger than the width at the heat source center. This means that the kerf width can be larger than $2D_F$. Strictly speaking, the thermal conduction effect should be taken into consideration even when the values D_F as well as D_S ahead of the beam axis are determined. In other words, the region in which the oxidation reaction can be maintained should be determined based not on the power density of the heat source but on the resultant temperature distribution. It should be noticed, however, that the kerf width is considerably close to $2D_F$ at a cutting speed range below 1 m/min. In the laser gas cutting in which materials are processed at high speeds with highly concentrated heat sources, the idea of the processing region limited by the power densities such as ϵ_S and ϵ_F is thought to be reasonable at the first approximation.

According to Ref. [13], it has been reported that the

cutting front activated by the laser beam moves forwards until it is out of range of the laser beam at the cutting speed 25 cm/min, and that at the cutting speeds above a critical value, 60 cm/min, the cutting becomes steady. It was found by the authors, however, that the distance over which the front progressed before the oxidation reaction ceases was limited within the range of the laser beam, and that the critical speed was about 200 cm/min, as aforementioned. Those discrepancies are thought to be caused by the facts that cutting speed, 25 cm/min, in Ref. [13] is extremely slow probably resulting in self-burning phenomenon as for the former, and that the cutting phenomena in the edge cutting are different from the normal cutting we adopted, as for the later.

4.2 Recommendation for smooth cutting

Since the contour of the cut surfaces is consisted of a series of circular arcs, the roughness of the cut surface is related to the pitch of the striations to some extent.

The pitch of the striations is proportional to the value $D_F - D_S$ and inversely proportional to the value $V_{r0} - V_b$ at cutting speeds higher than the self-burning limit. When the cutting speed increases, $(D_F - D_S)$ and $(V_{r0} - V_b)$ decrease, hence the pitch remains almost constant by mutual compensation. In detail, however, the value l_r in **Fig. 16(c)** is seen to increase faster at the earlier period and then to become almost constant so that the mean value of V_r is equal to V_{r0}. This means that the reaction speed is faster than the cutting speed V_b during only short period just after the circle for ϵ_S comes in contact with the cutting front and then the circle itself moves at V_b leaving rather smooth surface there. Thus the cut surfaces become smooth with increase in the cutting speed as shown in **Fig. 10**, when the other cutting conditions are all the same. On the other hand, it is obvious that the well focused beam with smaller value of $D_F - D_S$ will bring more smooth cuts at given cutting speed. Therefore, the application of focused beam with smaller spot diameter is strongly recommended, which is practically available by the laser beam with a fundamental transversed mode, TEM_{00}, and/or by a lens having a short focal length. In **Fig. 10**, the effect of short focal length lens on the cut surface roughness can be seen; then lens having shorter focal length, f=63.5 mm, is seen to give the smooth cut surface in the upper part, but rather rough cut surface in the lower part due to the short focus depth. Lenses with short focal length are generally adequate for cutting thin plates.

Higher power laser beam is also recommended for smooth cutting. In other words, for given thickness of plate, higher speed cutting with the higher power is better than lower speed cutting with the lower power. In **Fig. 6(b)**, a recommended cutting region for 1 KW laser is shown with III_A.

5. Summary

High speed movie films for the laser gas cutting mild steel indicated that the cutting phenomena varied periodically resulting in regularly spaced striations on the cut edges until the steady cutting was established at the cutting speeds above a critical value V_{r0}. Based on the information obtained from the cut appearances, motion of the cutting front observed in the films, the power density distribution in the focused beam and the temperature distribution in the cutting front, the mechanisms for the laser gas cutting mild steel are discussed. The results obtained are summarized as follows:

(1) At cutting speeds below V_{r0}, about 2 m/min, which is independent of the laser power, the reaction front moves at a speed equal to V_{r0} within the range where the laser beam power is high enough to activate the reaction, resulting in periodically changing cutting.

(2) At speeds higher than V_{r0}, the cutting phenomena become steady and the high power beam elevates the temperature at the cutting front so that the high speed cutting is achieved which could not ever been achieved by the oxy-acetylen cutting.

(3) With well focused intense beam qualified cuts with smooth surface are obtainable at rather higher cutting speeds.

References

1) Y. Arata and I. Miyamoto; "Generation and Applications of CW High Power CO_2 Gas Laser", Technol. Repts. Osaka Univ., Vol. 17 (1967) No.285
2) A.B.J. Sullivan and R.T. Houldcroft: "Gas-jet Laser Cutting", British W. J., Vol. 14 (1967) No.8, 443-446
3) F.W. Lunau and E.W. Paine: "CO_2 Laser Cutting", Weld. & Metal Fab., Jan. (1969), 9-14
4) M.M. Scheartz, "Laser Welding and Cutting", W.R.C. Bulletin, Nov. (1971), No. 167, 1-34
5) P.T. Houldcroft: "The Importance of the Laser for Cutting and Welding", Weld. and Met. Fab., Feb. (1972), 42-46
6) G. Brandt, K.D. Kegel and J.V. Hulle: "Einige Ergebnisse von Schneid-und Schweißversuchen mit einem 900 W CO_2 Laser", Schweissen und Schneiden, Vol. 24 (1972), H7
7) I.J. Spalding, "Lasers - Their Applications and Operational Requirements", Opt. and Laser Tech., Dec. (1974), 263-272
8) J.D. Russell: "The Development of the Laser as a Welding and Cutting", British Weld. Inst. Res. Bulletin, Vol, 16 (1975), 245-248
9) S. Roy: "A Comparative Surface Integrity Study of Laser Cutting with Other Conventional Cutting Technique", Sheet Metal Industries, Oct. (1977), 994-1014

10) J. Clarke and M.M. Steen: Proceedings of Laser '78 Conference, London, March (1978)
11) Y. Arata, S. Takeuchi and I. Miyamoto: "Fundamental Research of Laser Gas Cutting - I", Journal of High Temperature Society (in Japanese), Vol. 4 (1978), No. 2, 122-134
12) V.S. Kovalenko, Y. Arata, H. Maruo and I. Miyamoto: "Experimental Study of Cutting Different Materials with a 1.5 KW CO_2 Laser", Trans. of J.W.R.I., Vo. 7 (1978) No. 2, 101-112
13) M.J. Adams: "Gas Jet Laser Cutting", Proceeding of the Conference on Advance of Welding Process, The British Weld. Inst., April (1970), 140-146
14) K. Teske: "Contribution to the Explanation of Gas Cutting Process", Schweissen und Schneiden, Vol. 9 (1956), No. 8, 122-129
15) H. Hofe: "New Information on the Mechanism of Gas Cutting", Schweissen und Schneiden, Vol. 19 (1967), No. 5, 213-219
16) A.K. Ninburg: "Some Aspects of the Metal Combution Mechanism during Oxygen Cutting", Svar. Proiz., (1968), No. 2, 40-42